PCCP

PAPER

View Article Online
View Journal | View Issue

Check for updates

Cite this: *Phys. Chem. Chem. Phys.*, 2018, **20**, 21136

Softening to hardening of stretched diamondene nanotubes

Lei Wang, *[a] Kun Cai,*[b] Siyu Wei[a] and Yi Min Xie[b]

Received 22nd May 2018,
Accepted 20th July 2018

DOI: 10.1039/c8cp03243b

rsc.li/pccp

Diamondene, a carbon nanomaterial containing both sp^2 and sp^3 carbon atoms, is obtained by compressing two or more layers of graphene. By curving rectangular diamondene and matching the unsaturated C–C bonds on the two unbent edges, a nanotube is built. We build two diamondene nanotubes (DNTs) with different radii and test their strengths under uniaxial tension. From the stress–strain curves, we discover that DNTs exhibit softening followed by hardening. The mechanism is as follows: the bond lengths and bond angles impart different stiffnesses to the tube at different axial strains. Molecular dynamics simulations demonstrate that the feature of the softening–hardening process is independent of either the tube radii or the system temperature. The critical strain for the tensile strength of a DNT becomes lower at a higher temperature. This is caused by thermal vibration of the atoms in the tubes. At the same temperature, for a DNT with a larger radius, the value of critical strain is higher. These properties will be beneficial for the potential applications of DNTs in nanodevices.

Published on 06 August 2018. Downloaded by Australian National University on 1/10/2019 8:31:11 PM.

1. Introduction

Carbon, the sixth element in the periodic table, is one of the essential elements in living organisms. Carbon materials are abundant in the earth, and they are essential to various human functions. Hence, carbon materials attract attention constantly. Nowadays, the development of new carbon materials is still a challenge, but it is still a fairly attractive field. Besides naturally occurring carbon materials such as graphite and diamond, other carbon materials with special features are also available. For example, fullerenes (or carbon nanoballs), once predicted by Osawa,[1] were manufactured by Smalley *et al.* in 1985.[2] In 1991, Iijima fabricated carbon nanotubes.[3] In 2004, Geim *et al.*[4] obtained a single layer of graphite, *i.e.*, graphene. Currently, both carbon nanotubes and graphene have been successfully applied in various fields.[5–12]

A carbon atom has $2s^2 2p^2$ electron configuration. Fullerene as well as graphene can be considered as sp^2 carbon materials. However, diamond is an sp^3 carbon material. Due to the unique electron configuration of the carbon atom, it is assumed that stable carbon materials containing both sp^2 atoms and sp^3 atoms can exist. An increasing number of experiments have provided evidence for this prediction.[13–16] Among the sp^2/sp^3 composites, diamondene[17–22] has attracted more attention in recent years because of the current popular research involving two-dimensional materials.[23–27]

It has been found that by compressing two or more layers of graphene, diamondene can be formed when the neighboring layers are covalently bonded. Since the fourth covalent bond is not easily formed in carbon materials, the fabrication of diamondene needs extremely high pressures, *e.g.*, above 10 GPa[20,21] at room temperature. In diamondene formed from a double layer of graphene, sp^2 and sp^3 atoms are uniformly separated from each other. On the other hand, as a two-dimensional material, diamondene has relatively higher bending stiffness than graphene of the same size; therefore, it still exhibits high flexibility. According to these two characteristics, we believe that a nanotube can be fabricated by curving a rectangular diamondene ribbon and welding the unbent edges using a high-energy electron beam. This type of a new one-dimensional nanomaterial is called diamondene nanotube (DNT). Moreover, the buckling behavior of DNTs has been investigated by Cai *et al.*[28]

It should be noted that this type of DNT looks similar to but is quite different from the so-called prestressed multiwalled carbon nanotubes (PMWCNTs) with an interlayer distance less than the regular spacing of 0.34 nm.[29,30] In PMWCNTs, the distances between the adjacent layers are in the range of 0.22–0.29 nm; these values are larger than the cutoff value of 0.2 nm in REBO-style interatomic potential functions. This implies that the interactions between the carbon atoms in different layers are not covalent bonds. However, a covalent bond, with an equilibrium bond length of about 0.16 nm, links two carbon atoms on the inner and outer walls in the DNT configuration. Briefly, a DNT has different bond topology as compared to a PMWCNT.

[a] *Department of Engineering Mechanics, College of Mechanics and Materials, Hohai University, Nanjing 211100, China. E-mail: WangL@hhu.edu.cn*
[b] *Centre for Innovative Structures and Materials, School of Engineering, RMIT University, Melbourne, VIC, 3001, Australia. E-mail: Kuncai99@163.com*

This journal is © the Owner Societies 2018

Published on 06 August 2018. Downloaded by Australian National University on 1/10/2019 8:31:11 PM.

In this study, we focus on the thermal stability of a DNT and the strength of the tube stretched along the tube axis at a finite temperature. The mechanical properties of a DNT are investigated using the molecular dynamics simulation approach along with theoretical analyses. Some results can be used as guidelines for potential applications of this novel nanotube in flexible nanodevices.

2. Models and methodology

DNTs (n, m) can be considered as reshaped concentric double carbon nanotubes (n, m). For example, a DNT ((18, 18)), as shown in Fig. 1, is formed by reshaping two (18, 18) armchair carbon nanotubes. Such a DNT is also called an armchair DNT. In this study, two DNTs, namely, ((18, 18)) and ((26, 26)) are selected for performing strength tests; their radii are $\sim$1.25 nm and $\sim$1.80 nm, respectively. The length of ((18, 18)) is $\sim$8.29 nm and that of ((26, 26)) is $\sim$2.26 nm.

DNTs are placed in an *NVT* ensemble for free relaxation prior to applying tension. To reveal the temperature effect on the stability of unconstrained DNTs, the system temperatures are set to T = 1 K, 100 K, 200 K, 300 K, 600 K, and 900 K. For discussing the temperature effect on the tensile strength of DNTs, T = 1 K, 50 K, 100 K, 200 K, 300 K, 600 K, and 900 K are considered. Periodic boundary conditions are adopted along the three orthogonal directions.

Molecular dynamics calculations are carried out to test the stability and strength of DNTs. LAMMPS,[31] an open source code, is used to perform the calculations. In each calculation, the interaction among the carbon atoms in the DNT is estimated by the AIREBO potential.[32] The system is first reshaped by potential minimization.

After minimization, the system is placed in an *NPT* ensemble for 300–500 ps of relaxation with a time step of 0.001 ps. Furthermore, if necessary, the tube is stretched with a strain ratio of 6.12573×10^{-5} ps^{-1} in the *NPT* ensemble. Geometric mapping of the simulation box is adopted to provide deformation of DNTs. To estimate the stability of the nanostructure, the variation of potential energy (VPE) of the system can be calculated. In this study, VPE of a DNT is calculated during the relaxation or loading process.

3. Results and discussion

3.1 Thermal stability of a DNT at finite temperatures

Before testing the uniaxial tensile strength of DNTs, we discuss the thermal stability of a DNT, *e.g.*, ((26, 26)) at finite temperatures. First, the DNT is built and placed in an *NVT* ensemble with PPP boundary conditions. After not less than 300 ps of relaxation, we observe the configurations of the DNT. Meanwhile, to show the stability of the system, we draw the potential energy per atom during relaxation (Fig. 2). The value of the atom's potential energy tends to be stable after few picoseconds, *i.e.*, the curve becomes flat. From the axial views of the DNT at 300 ps at either 1 K or 300 K (the inset in Fig. 2), we can observe that the nanotube is regular and has no broken bonds. The final stable value of the potential energy per atom at 300 K is the maximum value among those of the four cases. The value at 1 K is slightly lower than that at 300 K. This difference is caused due to thermal-vibration-induced fluctuations of the potential energy per atom in the system.

As can be observed, for the curves of potential energy per atom with respect to higher temperatures, *e.g.*, 600 K or 900 K, longer time is required to obtain a stable value. Interestingly, the stable value at 900 K is the minimum among those of the four cases. We also find that a major drop in the potential energy occurs within the first 50 ps for the DNT at 900 K, which is much shorter than that for the DNT at 600 K. Hence, we believe that the nanotube experiences different variations in its configuration at different temperatures. To reveal this difference, we obtain snapshots of the nanotube at both the temperatures (Fig. 3). It is evident that the initial DNT, *i.e.*, at 0 ps is clearly

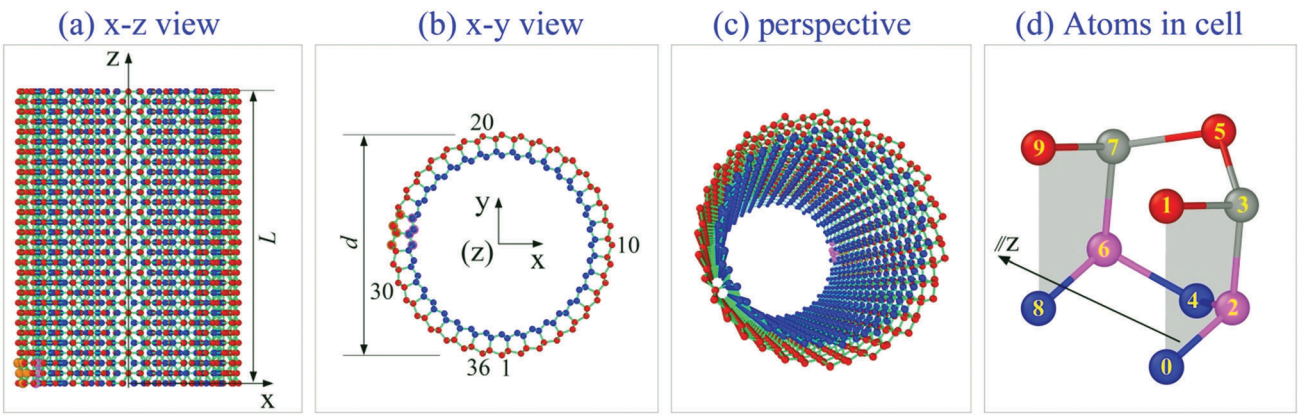

Fig. 1 A diamondene nanotube (DNT). (a–c) Views of DNT ((18, 18)) with length L and average diameter d and (d) representative atoms in the cell of a DNT. Atoms in blue or pink are on the inner surface of the DNT, and atoms in red or grey are on the outer surface. Both the surfaces are bonded by sp^3 carbon atoms (*e.g.*, atoms 2 and 6 in pink or 3 and 7 in grey). Atoms 0, 1, 4, 5, 8, and 9 are sp^2 atoms in DNT. Bonds 0–2, 2–3, and 1–3 are vertical to the z-axis.

Published on 06 August 2018. Downloaded by Australian National University on 1/10/2019 8:31:11 PM.

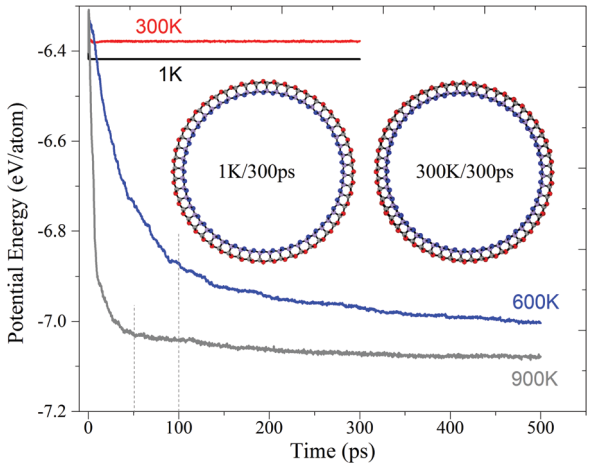

Fig. 2 Potential energy per atom in DNT ((26, 26)) during free relaxation at different temperatures.

bigger than that at 500 ps. Furthermore, the shape of the tube's cross-section varies with time. This demonstrates that the DNT shrinks at either 600 K or 900 K; in particular, the DNT is not stable at 900 K. For example, after 8 ps of relaxation, the column of sp^3–sp^3 bonds is broken (please see the defect in the orange frame). At 26 ps, a second defect appears. Before 500 ps, no further defects are generated. From the curves of the potential energy per atom, shown in Fig. 2, we can infer that the system tends to be in a stable state. Theoretically, the breakage of C–C bonds leads to an increase in the potential energy per atom. However, Fig. 2 shows that the system becomes more stable (*i.e.*, lower value of potential energy) at 900 K. The major reason for this is that the DNT has stronger shrinkage at 900 K than that at 600 K.

At 1 K, we also calculate the representative bond lengths and bond angles (Fig. 1d), and the results are shown in Fig. 4a and b, respectively. As bonds 1–3 and 0–2 are vertical to the tube axis, the values of l_{35} and l_{57} are identical; l_{24} and l_{46} tend to have the same value. Bonds (sp^3–sp^3) 2–3 and 6–7 are of equal length. Because the atoms of 1, 3, 5, and 7 are on the outer surface of the DNT and the remaining atoms are on the inner surface, the value of l_{13} ($\sim$0.1616 nm) is higher than the interlayer bond length, *i.e.*, $\sim$0.158 nm of l_{23}. The lowest length of the bond is observed for bond 0–2 because both atoms 0 and 2 are at the inner surface of the DNT. Moreover, the bond is vertical to the tube axis, which means that the bond is under the strongest compression. For the same reason of different curvatures of both the surfaces of the tube, bond angle α_{024} is much lower than α_{135}, but α_{246} is higher than α_{357} (Fig. 4b).

It is known that the interlayer bond length in diamondene[20] is $\sim$0.167 nm, and the C–C bond length in graphene is $\sim$0.142 nm. After comparing these two values, we find that all the present bond lengths (Fig. 4a) are between these values. Furthermore, l_{23} has a value of $\sim$0.158 nm, which is less than 0.167 nm, and it is under a compressive state. Bond l_{13} has a higher value than 0.155 nm (C–C bond length in diamond), which implies that it is under a tensile state. In particular, for bond 0–2, atom 0 is subjected to strong repulsion from its neighboring atoms within 1.0 nm (the cutoff of Lennard-Jones potential[33]). On the other hand, as bonds 1–3, 0–2, or 2–3 are vertical to the tube axis, their neighboring bonds 3–5 and 2–4 are easily broken than the other three types of bonds if the tube is under uniaxial tension (along the *z*-axis).

3.2 Strength of DNTs under uniaxial loading

Fig. 5 illustrates the variations in potential energy and axial stress of DNTs ((18, 18)) and ((26, 26)) during uniaxial stretching at finite temperatures. In LAMMPS, the local stress tensor of each atom is calculated based on a Virial-style definition.[34] Some essential conclusions can be drawn. First, for both the tubes, their critical strains are not more than 0.3, *i.e.*, the tube extends not more than 30% of its original length. Second, the critical strain of the DNT is lower at higher temperatures. Third, at temperatures below 300 K, the VPE curve (Fig. 5a or c) is smooth before approaching the corresponding critical strain. However, at higher temperatures, *e.g.*, 600 K or higher, VPE increases

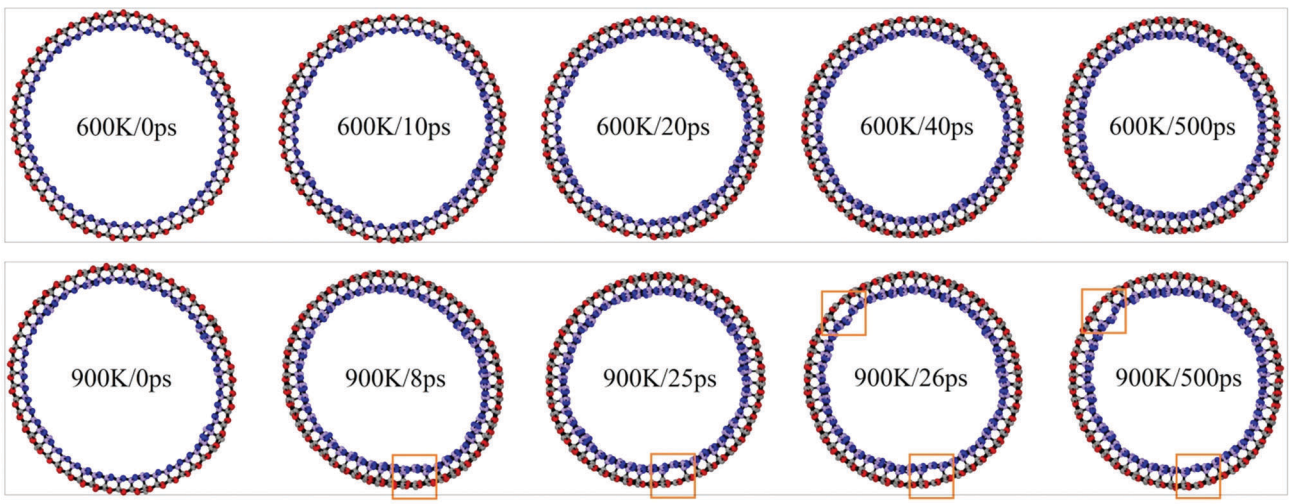

Fig. 3 Representative snapshots of DNT ((26, 26)) at different temperatures. The cutoff of C–C bonds is 0.2 nm.

 This journal is © the Owner Societies 2018

Published on 06 August 2018. Downloaded by Australian National University on 1/10/2019 8:31:11 PM.

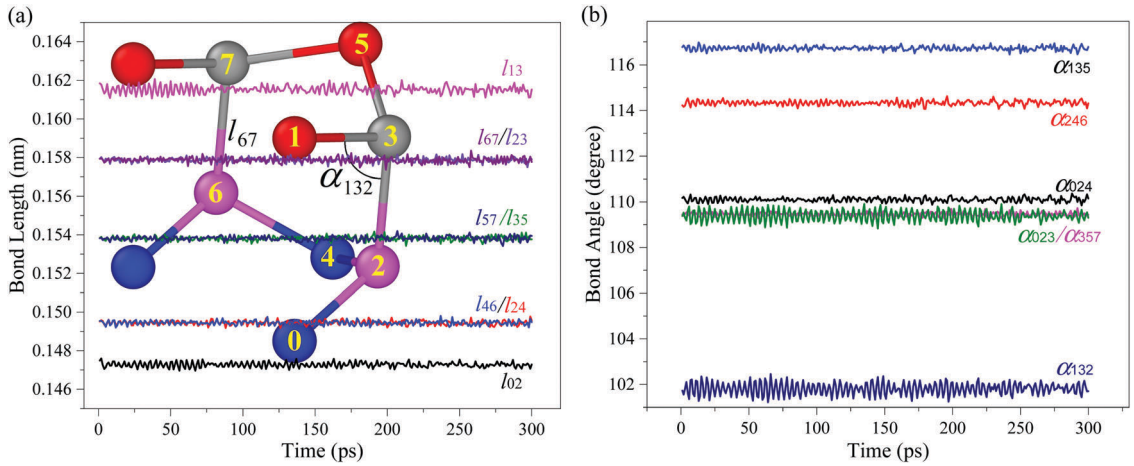

Fig. 4 Variation of bond length and bond angle for representative atoms in DNT ((26, 26)) during free relaxation when temperature is 1 K.

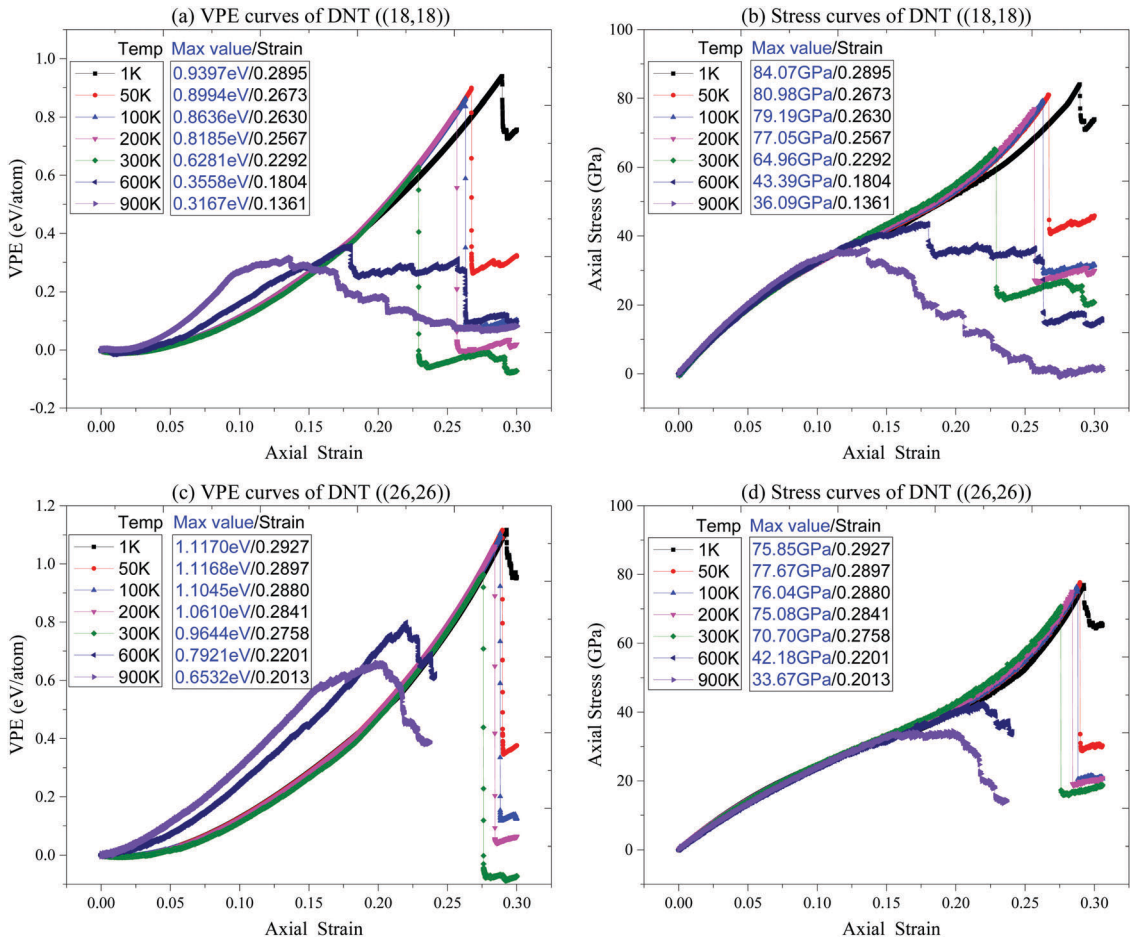

Fig. 5 Variation of potential energy and axial stresses of DNTs ((18, 18)) and ((26, 26)) under uniaxial stretching at different temperatures.

with fluctuations; besides, the related critical strain is clearly less than that at 300 K. It is necessary to demonstrate that both the tubes have different properties under the same uniaxial strain. Fourth, the tube ((26, 26)) has higher critical strain than the tube ((18, 18)) at the same temperature. For instance, at 300 K, the critical strains are ~0.2292 for ((18, 18)) and ~0.2758 for ((26, 26)). Lastly, for the tube with a higher radius, its critical strain reduces as the temperature increases from 1 K to 300 K.

As compared to VPE curves, the curves of the axial stress of both the tubes (Fig. 5b and d) reveal similar conclusions. For example, the critical stress with respect to the critical strain is higher at lower temperatures for the same tube; the critical

Published on 06 August 2018. Downloaded by Australian National University on 1/10/2019 8:31:11 PM.

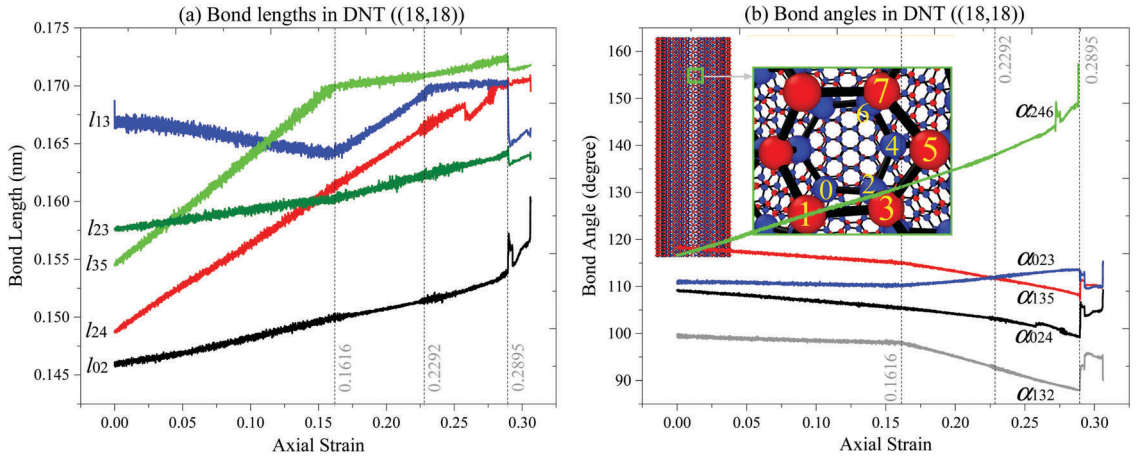

Fig. 6 Variation of representative bond lengths and bond angles in DNT ((18, 18)) under axial tension at 1 K.

stress at 300 K is much higher than that at 600 K or a higher temperature. However, at the same temperature, the critical stress of the slim tube ((18, 18)) is higher than that of ((26, 26)).

It is interesting that each stress curve with respect to temperatures below 300 K has two stages, *i.e.*, softening and hardening stages. For a lattice structure, both these stages should have different variations in the bond lengths and bond angles. To reveal this phenomenon, we draw the histories of the representative bond lengths and bond angles in the cell in DNT ((18, 18)) at 1 K, as shown in Fig. 6. The reason for choosing the tube at 1 K is that the thermal vibrations can be neglected, and the cross-section of the tube is only slightly different from a standard circular ring. Thus, the representative bonds can be easily selected.

From Fig. 6a, we find that the length of bond 1–3, *i.e.*, l_{13} undergoes three stages before the tube approaches the critical strain of 0.2895. As bond 1–3 is parallel to the *xy* plane and it belongs to the outer surface of DNT ((18, 18)), it is under tensile state before stretching of the tube. During stretching before the strain approaches 0.1616, l_{13} decreases; this implies that all the horizontal bonds at the outer surface of the tube reduce the axial stiffness of the stretched tube. When the strain is higher than 0.1616, l_{13} increases; this means that the bond starts to support the tensile load applied to the tube. However, after the axial strain reaches 0.2292, the length remains unchanged before the collapse of the tube.

Bond 3–5 also behaves uniquely during the stretching of the tube. For example, l_{35} increases to ~0.17 nm at the fastest growth rate among those of the five representative bonds before the axial strain approaches 0.1616; this is because this bond together with bond 5–7 has the smallest angle with the tube axis. During the stretching of the tube, the bonds cause the most resistance against deformation. Furthermore, the axial strain is mainly caused by the increase in the two types of bonds and the increase in their intersecting angles, *e.g.*, α_{357} (α_{246} in Fig. 6b); thereafter, it grows slowly.

Bond 2–4 belongs to the inner surface of the DNT and is not vertical to the tube axis. It is under compression before its length is less than 0.155 nm (C–C bond length in diamond). During the stretching of the tube, it grows faster than bond 0–2, which is vertical to the tube axis (the inset in Fig. 6b).

From the curves of the bond angles in Fig. 6b, it is observed that α_{246} increases, whereas α_{135} or α_{024} decreases. However, the angles related to the interlayer bonds, *e.g.*, α_{023} and α_{132} change differently. For example, after the axial strain reaches 0.1616, α_{023} increases, but α_{132} decreases. This is because atom 1 (sp^2 atom) is subjected to weaker repulsion from its neighboring nonbonding atoms when the tube is stretched long enough; *e.g.*, the strain is over 0.1616. Under weaker repulsion, atom 1 gets closer to the tube axis, but bond 2–3 is still along the radial direction. Hence, bond angle α_{132} is reduced at this stage. Atom 0 (sp^2 atom as well) is always under strong repulsion because it belongs to the inner surface of the tube, and the repulsion becomes stronger during stretching. Hence, α_{023} increases instead of decreasing.

Now, with respect to the curve of DNT ((18, 18)) at 1 K (Fig. 5b), we find that the softening of the axial stress ends at the axial strain of 0.1616. From the growing rates of l_{13} and l_{35} (Fig. 6a), the change in the radius of the DNT at this stage should be investigated. The radius of the outer surface of the tube can be estimated by the following equation:

$$R_o = \sim[l_{13} + l_{35} \times (-\cos\alpha_{135})] \times (18 + 18)/2\pi. \quad (1)$$

The related curve of R_o *vs.* axial strain is shown in Fig. 7a.

According to the curve of the tube radius (Fig. 7a), we know that the transversal shrinking of the stretched tube is slow at the softening stage. From Fig. 7b, we can observe that an increasing number of C–C bonds at the outer surface of the tube have lengths greater than 0.17 nm; *e.g.*, at strain of 0.2760, there are a few bonds at the outer surface (Fig. 8a), which means that the strength of the bonds becomes very weak. From previous analyses, we infer that most of the bonds are parallel to either bond 3–5 or bond 5–7. This conclusion is verified by the snapshots with respect to strain of 0.2292 (Fig. 8a). Some of the bonds at the inner surface of the tube are stretched longer than 0.17 nm until the axial strain is over 0.2760. Simultaneously, some interlayer bonds (sp^3–sp^3 bonds) become higher than 0.17 nm. However, this does not mean that the tube is broken,

 This journal is © the Owner Societies 2018

Published on 06 August 2018. Downloaded by Australian National University on 1/10/2019 8:31:11 PM.

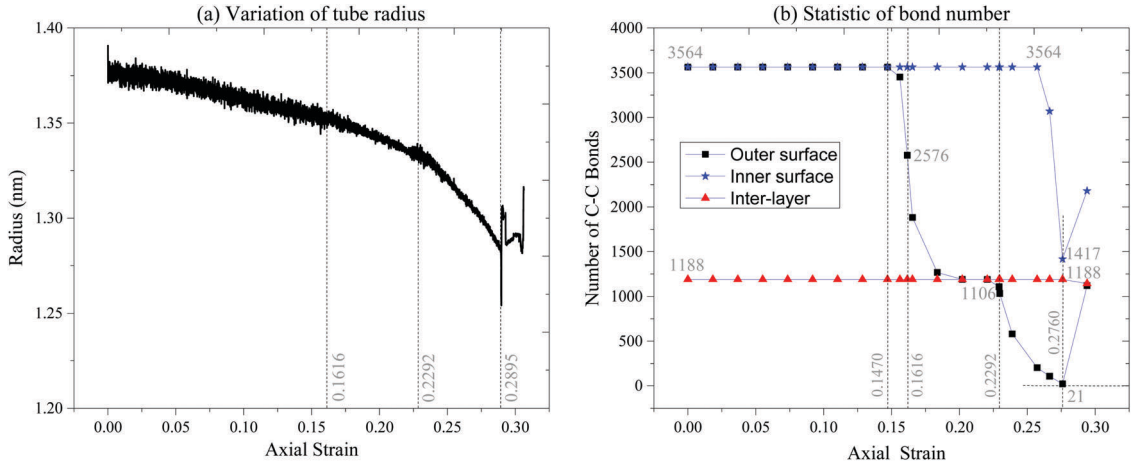

Fig. 7 Radius and bond number of DNT ((18, 18)) under uniaxial stretching at 1 K. Statistically, the cutoff of the bond is 0.17 nm.

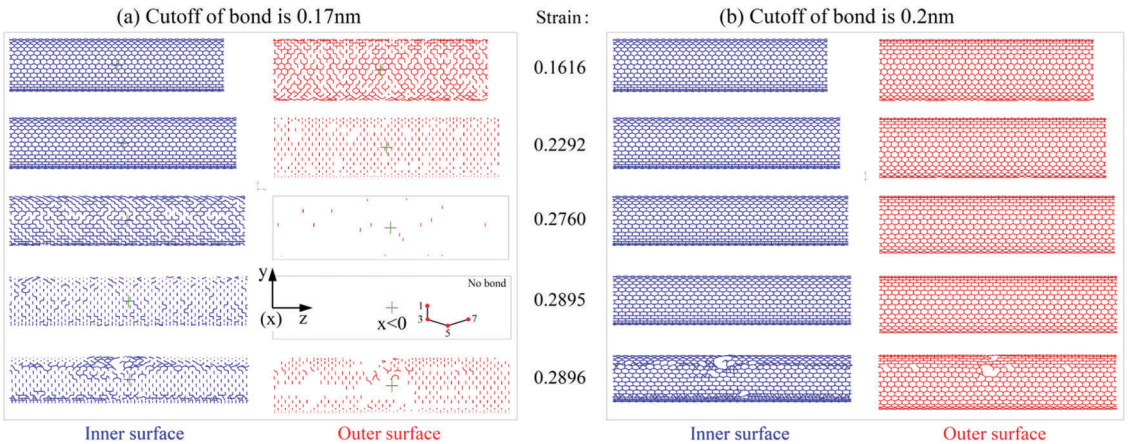

Fig. 8 Bond distributions in both the surfaces of the stretched DNT ((18, 18)) at 1 K. In these bonds, half side of the tube with respect to $x < 0$ is filtered by the slice in the *yz* plane. At strain of 0.2895, there is no bond in the outer surface in (a). However, when the cutoff of bond is set to be 0.2 nm, both inner and outer tubes remain undamaged until the strain reaches 0.2896, as shown in (b).

which implies that some bonds are longer than 0.2 nm and cannot return to their original state after the load is released; the snapshot at strain of 0.2896 in Fig. 8b may be referred. From this snapshot, we also find that the local breakage of the tube leads to stress release in the tube, and a larger number of bonds at the outer surface shrink to lengths shorter than 0.17 nm.

4. Conclusions

Diamondene is a carbon material containing sp^2 and sp^3 carbon atoms, and its physical properties are different from those of both graphene (sp^2) and diamond (sp^3). By curving a diamondene ribbon to form a nanotube, the thermal stability and tensile strength of the diamondene nanotube (DNT) are estimated. According to the molecular dynamics simulation results, the following conclusions are drawn for the potential usage of the new one-dimensional carbon material in nanodevices:

(1) After full relaxation in an *NVT* ensemble, a DNT with a radius of ~1.80 nm is stable at temperatures below 600 K, but it is not stable at 900 K due to the breakage of some sp^3–sp^3 bonds in the tube.

(2) In the unconstrained state, the sp^2–sp^3 bonds at the outer surface and vertical to the axis of an armchair DNT are under a tensile state; they are longer than the sp^3–sp^3 bonds. However, the sp^2–sp^3 bonds at the inner surface and vertical to the axis of the DNT are under a compressive state and have the shortest bond lengths.

(3) For either the longer ((18, 18)) or shorter ((26, 26)) DNT under uniaxial tension, the critical strain for the tensile strength is not more than 0.3. In particular, for a DNT with a lower radius, its critical strain is more sensitive to temperature than that of a DNT with a larger radius; at the same temperature, the former DNT has a lower value of the critical strain than the latter.

(4) The axial stress–strain curve of a DNT at a finite temperature illustrates that the DNT is initially in the softening state;

Published on 06 August 2018. Downloaded by Australian National University on 1/10/2019 8:31:11 PM.

after the axial strain increases beyond a threshold, *e.g.*, 0.1616 for DNT ((18, 18)) at 1 K, the tube turns into the hardening state when the temperature is not higher than 300 K.

(5) During the softening stage, the sp^2–sp^3 bonds at the outer surface and vertical to the axis of the DNT shrink and reduce the stiffness of the tube.

(6) At the hardening stage, all the bonds become longer during stretching of the tube. Meanwhile, an increasing number of oblique bonds, *i.e.*, the sp^2–sp^3 bonds at the outer surface but not vertical to the tube axis become longer than the bonds vertical to the tube axis; this is the reason for the hardening of the tube.

Briefly, the constitutive law of a DNT is nonlinear and temperature-dependent. While using a DNT in a flexible nanodevice, *e.g.*, a resonator, the features must impact the dynamic response of the nanodevice. In our future study, the potential applications of this new nanotube in such nanodevices will be discussed.

Conflicts of interest

The authors state that there is no competing financial interest.

Acknowledgements

The work is financially supported by National Natural Science Foundation, China (Grant No. 11472098), and National Key Research and Development Plan, China (Grant No. 2017YFC0405102).

References

1 E. Osawa, Superaromaticity, *Kagaku*, 1970, **25**, 854–863.
2 H. W. Kroto, J. R. Heath, S. C. Obrien, R. F. Curl and R. E. Smalley, C60: Buckminsterfullerene, *Nature*, 1985, **318**, 162–163.
3 S. Iijima, Helical microtubules of graphitic carbon, *Nature*, 1991, **354**, 56–58.
4 K. S. Novoselov, A. K. Geim, S. V. Morozov, D. Jiang, Y. Zhang, S. V. Dubonos, I. V. Grigorieva and A. A. Firsov, Electric field effect in atomically thin carbon films, *Science*, 2004, **306**, 666.
5 J. Cumings and A. Zettl, Low-friction nanoscale linear bearing realized from multiwall carbon nanotubes, *Science*, 2000, **289**, 602–604.
6 A. Barreiro, R. Rurali, E. R. Hernandez, J. Moser, T. Pichler, L. Forro and A. Bachtold, Subnanometer motion of cargoes driven by thermal gradients along carbon nanotubes, *Science*, 2008, **320**, 775–778.
7 K. Cai, H. Yin, Q. H. Qin and Y. Li, Self-excited oscillation of rotating double-walled carbon nanotubes, *Nano Lett.*, 2014, **14**, 2558–2562.
8 S. H. Kim, C. S. Haines, N. Li, K. J. Kim, T. J. Mun, C. S. Choi, J. T. Di, Y. J. Oh, J. P. Oviedo, J. Bykova, S. L. Fang, N. Jiang, Z. F. Liu, R. Wang, P. Kumar, R. Qiao, S. Priya, K. Cho, M. Kim, M. S. Lucas, L. F. Drummy, B. Maruyama, D. Y. Lee, X. Lepró, E. Gao, D. Albarq, R. Ovalle-Robles, S. J. Kim and R. H. Baughman, Harvesting electrical energy from carbon nanotube yarn twist, *Science*, 2017, **357**, 773–778.
9 S. V. Morozov, K. S. Novoselov, M. I. Katsnelson, F. Schedin, D. C. Elias, J. A. Jaszczak and A. K. Geim, Giant intrinsic carrier mobilities in graphene and its bilayer, *Phys. Rev. Lett.*, 2008, **100**, 016602.
10 R. R. Nair, P. Blake, A. N. Grigorenko, K. S. Novoselov, T. J. Booth, T. Stauber, N. M. Peres and A. K. Geim, Fine structure constant defines visual transparency of graphene, *Science*, 2008, **320**, 1308.
11 X. F. Xu, L. F. C. Pereira, Y. Wang, J. Wu, K. W. Zhang, X. M. Zhao, S. K. Bae, C. T. Bui, R. G. Xie, J. D. L. Thong, B. H. Hong, K. P. Loh, D. Donadio, B. W. Li and B. Ozyilmaz, Length-dependent thermal conductivity in suspended single-layer graphene, *Nat. Commun.*, 2014, **5**, 3689.
12 M. Y. Zhong, D. K. Xu, X. G. Yu, K. Huang, X. M. Liu, Y. M. Qu, Y. Xu and D. R. Yang, Interface coupling in graphene/fluorographene heterostructure for high-performance graphene/silicon solar cells, *Nano Energy*, 2016, **28**, 12–18.
13 A. P. M. Barboza, M. H. D. Guimaraes, D. V. P. Massote, L. C. Campos, N. M. Barbosa Neto, L. G. Cancado, R. G. Lacerda, H. Chacham, M. S. C. Mazzoni and B. R. A. Neves, Room-temperature compression-induced diamondization of few-layer graphene, *Adv. Mater.*, 2011, **23**, 3014–3017.
14 S. Rajasekaran, F. Abildpedersen, H. Ogasawara, A. Nilsson and S. Kaya, Interlayer carbon bond formation induced by hydrogen adsorption in few-layer supported graphene, *Phys. Rev. Lett.*, 2013, **111**, 085503.
15 D. Odkhuu, D. Shin, R. S. Ruoff and N. Park, Conversion of multilayer graphene into continuous ultrathin sp^3-bonded carbon films on metal surfaces, *Sci. Rep.*, 2013, **3**, 3276.
16 J. W. Jiang, J. Leng, J. Li, Z. Guo, T. Chang, X. Guo and T. Zhang, Twin graphene: a novel two-dimensional semiconducting carbon allotrope, *Carbon*, 2017, **118**, 370–375.
17 Y. Y. Zhang, C. M. Wang, Y. Cheng and Y. Xiang, Mechanical properties of bilayer graphene sheets coupled by sp^3 bonding, *Carbon*, 2011, **49**, 4511–4517.
18 J. Li, H. Li, Z. Wang and G. Zou, Structure, magnetic, and electronic properties of hydrogenated two-dimensional diamond films, *Appl. Phys. Lett.*, 2013, **102**, 073114.
19 A. R. Muniz, A. S. Machado and D. Maroudas, Mechanical behavior of interlayer-bonded nanostructures obtained from bilayer graphene, *Carbon*, 2015, **81**, 663–677.
20 L. G. P. Martins, M. J. S. Matos, A. R. Paschoal, P. T. C. Freire, N. F. Andrade, A. L. Aguiar, J. Kong, B. R. A. Neves, A. B. de Oliveira, M. S. C. Mazzoni, A. G. S. Filho and L. G. Cançado, Raman evidence for pressure-induced formation of diamondene, *Nat. Commun.*, 2017, **8**, 96.
21 Y. Gao, T. F. Cao, F. Cellini, C. Berger, W. A. de Heer, E. Tosatti, E. Riedo and A. Bongiorno, Ultrahard carbon film from epitaxial two-layer graphene, *Nat. Nanotechnol.*, 2018, **13**, 133–138.
22 J. Shi, K. Cai and Y. M. Xie, Thermal and tensile properties of diamondene at finite temperature: a molecular dynamics study, *Mater. Des.*, 2018, **156**, 125–134.

 This journal is © the Owner Societies 2018

Published on 06 August 2018. Downloaded by Australian National University on 1/10/2019 8:31:11 PM.

23 L. K. Li, Y. J. Yu, G. J. Ye, Q. Q. Ge, X. D. Ou, H. Wu, D. L. Feng, X. H. Chen and Y. B. Zhang, Black phosphorus field-effect transistors, *Nat. Nanotechnol.*, 2014, **9**, 372–377.
24 J. W. Jiang and H. S. Park, Negative poisson's ratio in single-layer black phosphorus, *Nat. Commun.*, 2014, **5**, 4727.
25 T. Jakubczyk, K. Nogajewski, M. R. Molas, M. Bartos, W. Langbein, M. Potemski and J. Kasprzak, Impact of environment on dynamics of exciton complexes in a WS_2 monolayer, *2D Mater.*, 2017, **5**, 031007.
26 D. J. Late, B. Liu, H. S. Matte, V. P. Dravid and C. N. Rao, Hysteresis in single-layer MoS_2 field effect transistors, *ACS Nano*, 2012, **6**, 5635–5641.
27 L. Song, L. J. Ci, H. Lu, P. Sorokin, C. H. Jin, J. Ni, A. G. Kvashnin, D. G. Kvashnin, J. Lou, B. I. Yakobson and P. M. Ajayan, Large scale growth and characterization of atomic hexagonal boron nitride layers, *Nano Lett.*, 2010, **10**, 3209–3215.
28 K. Cai, L. Wang and Y. M. Xie, Buckling behavior of nanotubes from diamondene, *Mater. Des.*, 2018, **149**, 34–42.
29 H. W. Zhang, L. Wang and J. B. Wang, Computer simulation of buckling behavior of double-walled carbon nanotubes with abnormal interlayer distances, *Comput. Mater. Sci.*, 2007, **39**, 664–672.
30 Z. P. Xu, L. F. Wang and Q. S. Zheng, Enhanced mechanical properties of prestressed multi-walled carbon nanotubes, *Small*, 2008, **4**, 733–737.
31 LAMMPS, Molecular Dynamics Simulator, http://lammps.sandia.gov/, retrieved May 18, 2018.
32 S. J. Stuart, A. B. Tutein and J. A. Harrison, A reactive potential for hydrocarbons with intermolecular interactions, *J. Chem. Phys.*, 2000, **112**, 6472–6486.
33 J. E. Jones, On the determination of molecular fields: II. From the equation of state of a gas, *Proc. R. Soc. London*, 1924, **106**, 463–477.
34 A. P. Thompson, S. J. Plimpton and W. Mattson, General formulation of pressure and stress tensor for arbitrary many-body interaction potentials under periodic boundary conditions, *J. Chem. Phys.*, 2009, **131**, 154107.